ADVANCED QUANTUM TECHNOLOGIES
www.advquantumtech.com

Theory of Center-Line Slope in 2D Electronic Spectroscopy with Static Disorder

Zong-Hao Sun, Yi-Xuan Yao, Qing Ai, and Yuan-Chung Cheng**

2D electronic spectroscopy (2DES) is a powerful tool for investigating the dynamics of complex systems. However, analyzing the resulting spectra can be challenging, and thus may require the use of theoretical modeling techniques. The center-line slope (CLS) method is one of such approaches, which aims to extract the time correlation function (TCF) from 2DES with minimal error. Since static disorder is widely observed in complex systems, it may be interesting to ask whether the CLS approach still work in the presence of the static disorder. In this paper, the effect of the static disorder on the TCF obtained through the CLS method is investigated. It is found that the steady-state value of the CLS increases monotonically with respect to the static disorder, which suggests that the amplitude of the static disorder can be determined using the CLS in the long-time limit. Additionally, as the static disorder rises, the decay rate of the CLS first decreases to a certain value and remains at this value until the static disorder is sufficiently large. Afterward, the CLS begins to fluctuate significantly and thus results in obtaining the decay rate through the CLS method unreliable. Based on these discoveries, the authors propose a method to fix the error and obtain the TCF.
The findings may pave the way for obtaining reliable system-bath information by analyzing 2DES in the practical situations.

1. Introduction

2DES is a powerful spectral technology developed in recent years for analyzing the dynamics of a variety of chemical and biological systems.[1–9] It has high resolution in both time and frequency domains, and has been successfully applied to probing fast dynamics in condensed-matter systems with exceptional detail. The 2DES is a branch of the 2D spectroscopy in the visible domain, which is widely used in the study of photoactive systems including photosynthetic complexes,[10–16] photovoltaics,[17,18] nanocrystalline,[19–21] quantum dots and wells,[22–24] and photosynthetic pathways.[25–28] The nonlinear broadening, energy transfer, electron-vibration coupling effects and quantum coherence effects can be intuitively demonstrated in the 2DES. Several closely-related technologies have also been developed, such as 2D fluorescence spectroscopy[29–31] and 2D terahertz.[32,33]

In the 2DES experiments, three ultrafast pulses covering the frequency domain of interest successively pass the sample. By controlling the delay times of the pulses, a photon-echo signal is emitted in the direction of phase matching after the interaction between three pulses and the sample. The photon-echo signal is combined with another local-oscillator signal for heterodyne detection, which provides the amplified signal for the quantum dynamics.

The first coherence period τ is the duration between the first two pulses. The population period T_w is the duration between the second and third pulses. The second coherence period t is the duration between the third pulse and the signal. They can be effectively adjusted by tuning the delay times of the pulses. The electrons are labeled by frequency during the first coherence period. Due to the microscopic events that occur during the population period, the frequency-labeled electrons may develop to various frequencies, that is, the spectral diffusion. The final frequencies of the electrons with frequency labels are read out during the second coherence period. By taking the initial frequency which labels the electrons as one axis and the final frequency as the other axis, a 2D spectrum can be obtained. The detailed information and quantum dynamics of the system can be determined by analyzing the position, amplitude and shape of the peaks in the 2D spectrum.

2DES contains immense information about the system. It is crucial how to interpret the spectrum to obtain the required information. In order to explore the dynamic evolution of the system, we focus on extracting the TCF accurately and efficiently from the 2D spectrum. The TCF provides a key connection between 2DES photon-echo experiments and microscopic dynamics. Hence, many methods have been developed, such as the CLS,[34,35] ellipticity and eccentricity.[36,37]

Among methods for extracting information describing the system-bath interaction, the CLS theory yields reliable TCF and has been successfully applied to describe 2D infrared vibrational echo spectroscopy and structural dynamics under thermal equilibrium.[38,39] The CLS is the slope (the inverse of the slope) of

Z.-H. Sun, Y.-X. Yao, Q. Ai
Department of Physics, Applied Optics Beijing Area Major Laboratory
Beijing Normal University
Beijing 100875, China
E-mail: aiqing@bnu.edu.cn
Y.-C. Cheng
Department of Chemistry and Center for Quantum Science and Engineering
National Taiwan University
Taipei 106, Taiwan
E-mail: yuanchung@ntu.edu.tw
The ORCID identification number(s) for the author(s) of this article can be found under https://doi.org/10.1002/qute.202300163

DOI: 10.1002/qute.202300163

the center line that connects the peaks of a series of cuts through the 2D spectrum parallel to the ω_t (ω_τ) axis. As spectral diffusion progresses, the CLS decays from a maximum of 1 to 0. The CLS is used as the TCF to study the ultrafast dynamics of the system.

The CLS theory is developed based on the theory of optical response function.[40,41] In the derivation, the TCF is assumed as a real function, and many approximation methods have been applied, such as the short-time approximation, which may significantly deviate from the practical situation.

In order to apply the CLS method more accurately to real-world situations, numerous studies have been conducted. Šanda and colleagues investigated the relationship between the CLS shapes and solvent effects, vibrational dissipation, and peak positions.[42] Hoffman and co-workers attempted to determine TCF parameters quickly and accurately using artificial neural networks.[43] However, static disorder may be a significant factor influencing spectral features, particularly in complex systems. The impact of static disorder on the interpretation and analysis of 2DES warrants further investigation.

In natural photosynthetic complexes, the TCF is complex and can only be considered as a real function at the high-temperature limit.[40] As a result, it might be crucial to test the reliability of the CLS approach when the TCF is a complex function. On the other hand, due to the heterogeneity, the inhomogeneous broadening is introduced due to the static disorder and it may effectively prolong the coherence signals in the 2DES.[44,45] Therefore, it might be important to investigate the effects of the static disorder on the CLS. Interestingly, it is found that within a certain range of the static disorder, the performance of the CLS approach has been improved in extracting the TCF.

This paper is organized as follows. In the next section, we give a brief introduction to the optical response function for 2DES and the CLS method. In Section 2, we examine the performance of the CLS method at low temperatures. Using complex TCF, we generate 2D spectra at 77 and 298 K, respectively. In Section 3, we calculate 2DES with the static disorder and investigate its impact on the CLS method. In Section 4, we summarize our main findings. In Supporting Information, we provide a brief derivation to the probability of the energy gap in the presence of the static disorder. In Supporting Information, we also derive the relation between the real and imaginary parts of the TCF.

2. CLS at Low Temperature

In the original CLS approach, a real function is assumed for the TCF. It can be viewed as the high-temperature limit of the natural photosynthetic complexes. In this section, we will test the reliability of the CLS approach at a low temperature, that is, a complex function[46] $C(t) = C'(t) - iC''(t)$, where

$$C'(t) = \frac{1}{\pi}\int_0^\infty \mathrm{d}\omega\, J(\omega)\coth\left(\frac{\beta\omega}{2}\right)\cos(\omega t)$$
$$C''(t) = \frac{1}{\pi}\int_0^\infty \mathrm{d}\omega\, J(\omega)\sin(\omega t) \quad (1)$$
$$J(\omega) = \gamma_c\omega\exp(-\omega/\omega_c)$$

Table 1. Parameters of the TCF at $T = 298$ K for an Ohmic spectral density with cutoff 40 cm^{-1} and $\gamma_c = 1$.

TCF	α_k ($\times 10^2\,\mathrm{fs}^{-2}$)	$\mathrm{Re}(\gamma_k)$ ($\times 10^{-3}\,\mathrm{fs}^{-1}$)	$\mathrm{Im}(\gamma_k)$ ($\times 10^{-3}\,\mathrm{fs}^{-1}$)
$C'(t)$	65.24	9.183	0
$C'(t)$	9.001	2.336	0
$C'(t)$	−10.56	28.62	19.17
$C'(t)$	−10.56	28.62	−19.17
$C''(t)$	−0.9246	6.374	−5.870
$C''(t)$	−0.9246	6.374	5.870
$C''(t)$	2.655	20.76	−20.48
$C''(t)$	2.655	20.76	20.48
$C''(t)$	−3.717	5.360	0

Table 2. Parameters of the TCF at $T = 77$ K for an Ohmic spectral density with cutoff 40 cm^{-1}, and $\gamma_c = 1$.

TCF	α_k ($\times 10^3\,\mathrm{fs}^{-2}$)	$\mathrm{Re}(\gamma_k)$ ($\times 10^{-3}\,\mathrm{fs}^{-1}$)	$\mathrm{Im}(\gamma_k)$ ($\times 10^{-5}\,\mathrm{fs}^{-1}$)
$C'(t)$	11.82	17.51	−2.777
$C'(t)$	11.82	17.51	2.777
$C'(t)$	−22.64	18.40	0
$C'(t)$	0.4852	3.331	0
$C''(t)$	−2.879	23.77	−3.043
$C''(t)$	−2.879	23.77	3.043
$C''(t)$	3.022	24.08	−781.9
$C''(t)$	3.022	24.08	781.9
$C''(t)$	−0.2854	5.595	0

Here, the relationship between the TCF and the Ohmic spectral density is provided, where γ_c characterizes the system-bath coupling strength. The cutoff frequency ω_c is introduced to limit the influence of high-frequency vibrations, while $\beta = 1/(k_B T)$ represents the inverse temperature. Alternatively, the real and imaginary parts of the TCF are given as

$$C'(t) = \sum_k \alpha_k e^{-\gamma_k t}$$
$$C''(t) = \sum_k \alpha_k e^{-\gamma_k t} \quad (2)$$

Table 1 shows the parameters of the complex function when the temperature is 298 K. The real and imaginary parts of the TCF should satisfy the corresponding relation Equation (8). We also consider the case of a low temperature, for example, 77 K, with parameters given in **Table 2**.

As schematically depicted in **Figure 1**, we use a configuration of a dimer with coupling strength J for calculation, where the two-exciton state has been neglected. In **Figure 2**, we show the diagonal peaks with lower energy in the absorptive 2DES generated from the response function. The red (blue) solid lines in the diagram are the center lines for ω_t (ω_τ). In the neighborhood of the peak, these two lines are very close to a straight line, and their slopes are the CLS. In order to obtain the behavior of the TCF in the time domain, we calculate the 2DES for a series of waiting times T_w. With the increase of T_w, the shape of the peak changes from ellipse to circle due to the spectral diffusion.[35] Moreover, in

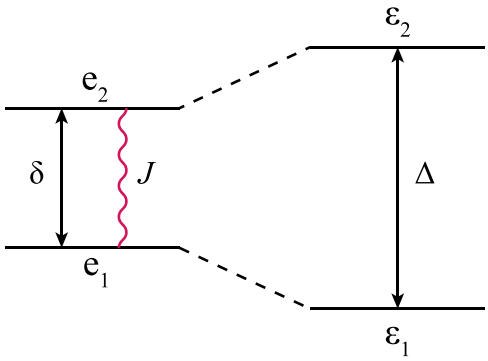

Figure 1. The dimer system with coupling strength J, where $\epsilon_1 = 15\,800\ \mathrm{cm}^{-1}$, $\delta \equiv \epsilon_2 - \epsilon_1 = 400\ \mathrm{cm}^{-1}$ is the energy gap between $|e_2\rangle$ and $|e_1\rangle$. When there is resonant coupling $J = 150\ \mathrm{cm}^{-1}$ between $|e_2\rangle$ and $|e_1\rangle$, the energy gap has been widened as $\Delta = \sqrt{\delta^2 + 4J^2}$.

the long-time limit, the two center lines tend to be parallel to the two coordinate axes respectively. According to the CLS approach, since the slopes of the two lines gradually approach 0, the TCF eventually vanishes.

Notice that when it is far away from the peak, the center line significantly deviates from a straight line. In order to effectively obtain the TCF, we restrict the center line to the full width at the half maximum (FWHM) of the peak and numerically fit it to obtain the CLS. The relation between the CLS and the waiting time T_w is shown in **Figure 3**, where the CLS is normalized by its value at $T_w = 0$ fs. Notice that the CLSω_t and CLSω_τ coincide with each other for the whole parameter regime. When the temperature is high, that is, $T = 298$ K in Figure 3a, the CLS decays faster than the TCF at the initial stage, while it will be surpassed around $T_w = 200$ fs. However, when the temperature is lowered to $T = 77$ K in Figure 3b, the situation becomes subtle although the tendency remains almost the same. The CLSω_t and CLSω_τ begin to move apart after $T_w = 500$ fs. The underlying physical mechanism will be discussed in the next section.

3. The Effect of Static Disorder on the CLS

As shown in Figure 1, in order to consider the effects of the static disorder, we calculate the 2DES with the level spacing δ characterized by a Gaussian distribution with mean zero and standard deviation σ. Assuming there is electronic coupling J between the two levels, the probability of the energy gap Δ between the two eigenstates as

$$P(\Delta) = \frac{\exp\left(-\frac{(\sqrt{\Delta^2-J^2}-\omega_{eg}^0)^2}{4\sigma_D^2}\right) + \exp\left(-\frac{(\sqrt{\Delta^2-J^2}+\omega_{eg}^0)^2}{4\sigma_D^2}\right)}{\sqrt{4\pi}\sigma_D \Delta^{-1}\sqrt{\Delta^2 - J^2}} \tag{3}$$

which is derived in Supporting Information. In the paper, we use the 128-point Gauss–Hermite quadrature method[47] to calculate the spectra for each waiting time T_w.

For static disorder in the range 10–200 cm^{-1}, we calculate the 2DES and obtain the corresponding CLS. We find that the 2DES is modified mainly in three aspects due to the static disorder, that is, the shape of the spectral peak, the steady-state value of the CLS in the long-time limit and the decay rate γ of the CLS.

3.1. The Shape of Spectral Peak

In **Figure 4**, we show the 2DES of $T_w = 10$ fs for three typical static disorders. Compared with Figure 2b, the peak has been stretched along the diagonal line as a result of the static disorder. With the increase of the static disorder, the stretching effect becomes more significant. Notice that when the static disorder is greater than 130 cm^{-1}, a series of smaller peaks with lower height emerge in the diagonal line and the center line appears wavy, which is significantly different from a straight line. This effect will significantly affect the acquisition of the CLS, making it difficult to obtain the TCF. It is worth noting that the impact of the static disorder is greater at the case that $T = 77$ K compared to $T = 298$ K. For example, at $\sigma = 130\ \mathrm{cm}^{-1}$, the spectrum at $T = 298$ K is affected by the static disorder causing the peak shape to be stretched along the diagonal direction. However, the stretching effect at $T = 77$ K is more intense, splitting into multiple smaller peaks along the diagonal direction. A similar effect does not appear in the 298 K graph until σ increases to 190 cm^{-1}.

We remark that the emergency of the lower peaks is due to the finite order of the Gauss–Hermit method, which is utilized to simulate the static disorder. This defect can be overcome by increasing the order and thus results in raising the computational cost.

3.2. The Steady-State Value of the CLS

Another effect of the static disorder is reflected in the steady-state value of the CLS in long-time limit. In the absence of the static disorder, the steady-state value of the CLS goes to 0, which is the same as the behavior of the TCF. However, we find that when the static disorder is introduced, the CLS at the steady state no longer vanishes. This steady-state value increases when the amplitude of the static disorder is enlarged.

Figure 5 shows the change of the steady-state value with the static disorder. We find that there is a monotonic relation between the steady-state value of the CLS and the amplitude of the static disorder. As the latter increases, the steady-state value of the CLS increases rapidly. When δ raises to 50 cm^{-1}, the CLS ultimately decays only to ≈70% of its initial value. At a temperature of 298 K, the steady-state values of CLSω_τ and CLSω_t overlap with each other in whole parameter regime, as shown in Figure 5a. However, at a lower temperature of 77 K as shown in Figure 5b, when σ exceeds 140 = cm^{-1}, an abnormal fluctuation in the steady-state values of CLSω_τ and CLSω_t appears at 77 K. We speculate that this is due to the excessive impact of static disorder on the peak shape, causing the CLS method to fail to extract information correctly. In comparison to the situation at 77 K, at 298 K a similar fluctuation does not appear in Figure 5a.

3.3. The Decay Rate of the CLS

The static disorder also affects the decay rate of the CLS. For a group of spectra with different T, we perform a single exponential fitting, that is, in the form of $ae^{-\gamma t} + b$, to obtain the decay rate γ of the CLS, which is very crucial in studying open quantum dynamics. The actual TCF, as shown in Equation (2), is the

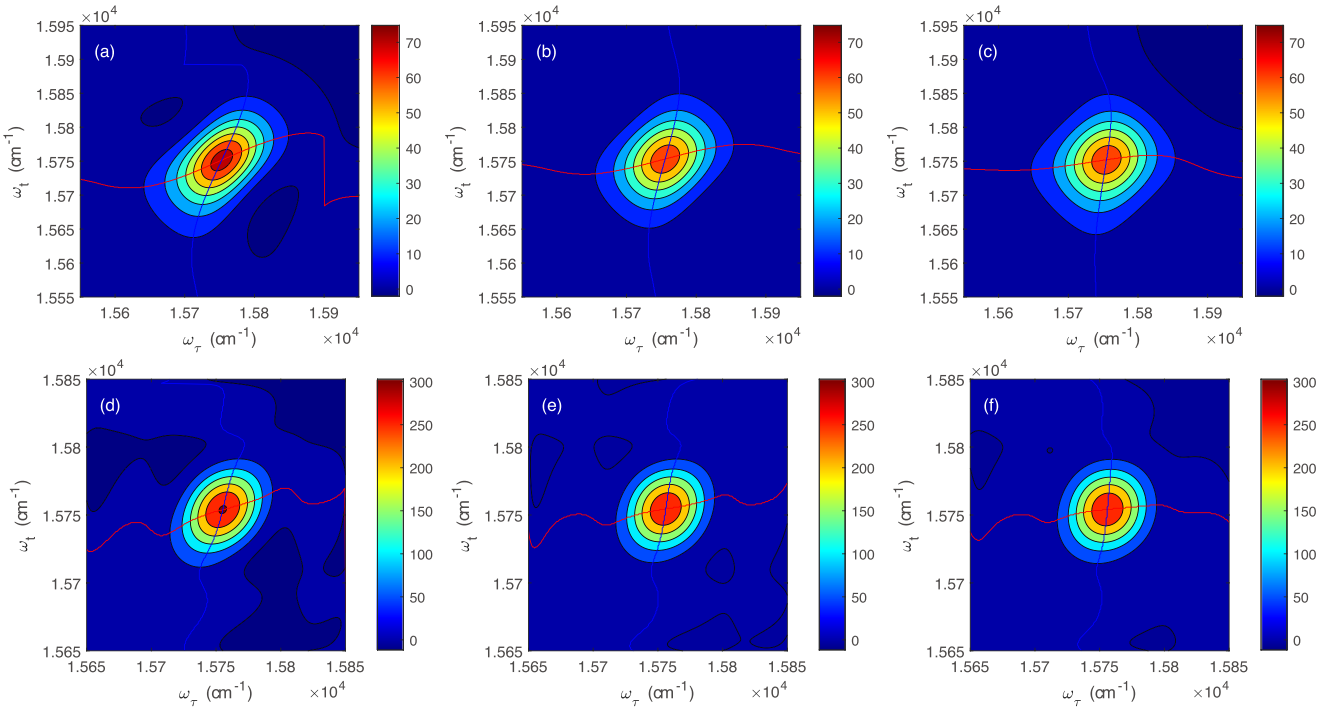

Figure 2. Absorptive 2DES simulated from the response function at the waiting time a,d) T_w = 10 fs; b,e) 100 fs; and c,f) 200 fs. The red (blue) solid line is the center line for ω_t (ω_τ). The sub-figures (a– c) are simulated with T = 298 K, while (d–f) with T = 77 K.

sum of multiple exponential functions, but fitting data with multiple exponential functions may result in many possible sets of fitting results due to too many parameters, which is not helpful in obtaining information about the interaction between the system and the environment. As von Neumann said,[48,49] "With four parameters I can fit an elephant, and with five I can make him wiggle his trunk." Therefore, we use a single exponential function for fitting, which may not perfectly match the data, but can capture the main decay component of the TCF and provide the dominant interaction component between the system and the environment.

Figure 6 shows the decay rate of the CLS under different static disorders, where the black dashed line is the decay rate of the TCF. We find that at both temperatures, that is, 298 and 77 K, the decay rate of the CLS exhibits a similar relation with the amplitude of static disorder. After the static disorder emerges, as it increases, the decay rate of the CLS decreases, causing the decay to slow down. When the decay rate decreases to a certain value, it stops decreasing and remains as a constant regardless of the increasing static disorder. In Figure 6a, as the static disorder is larger than about 130 cm^{-1}, the decay rate begins to fluctuate. When σ increases to nearly 200 cm^{-1}, the CLS theory fails to

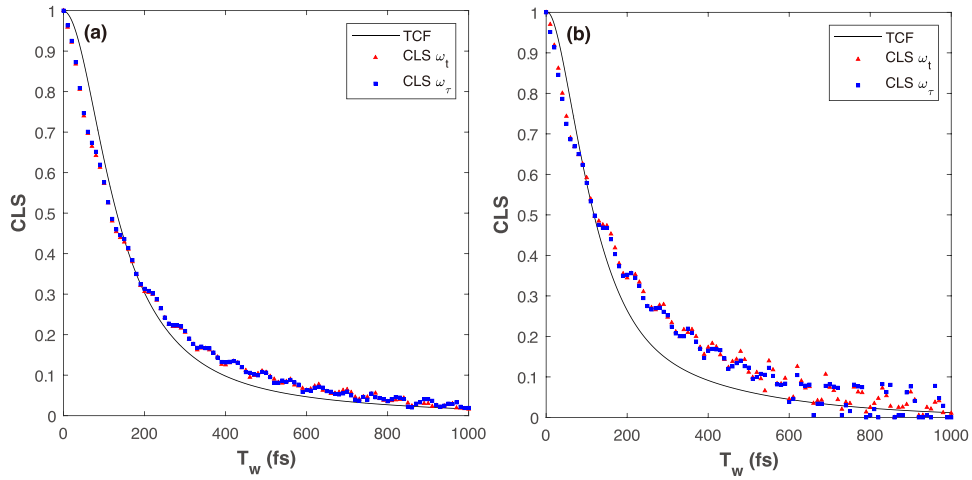

Figure 3. The dependence of the CLS on the waiting time T_w, where CLS is simulated at a) T = 298 K, b) T = 77 K. The black line is the real part of the TCF.

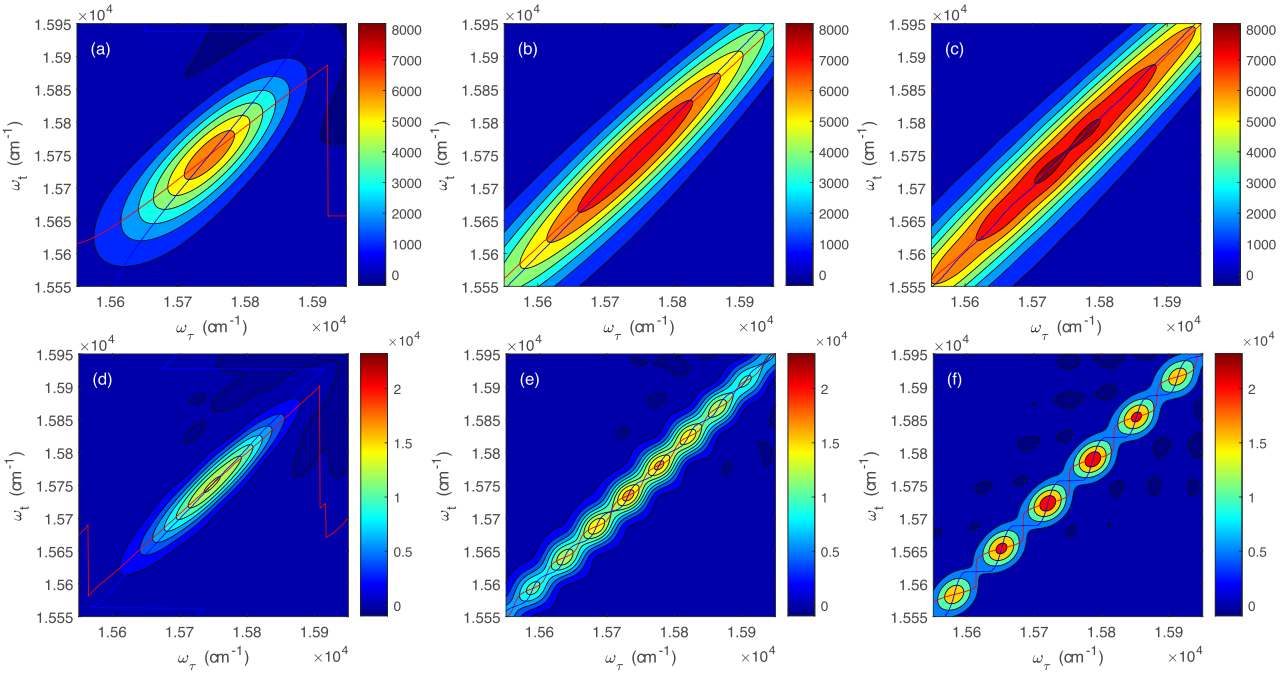

Figure 4. Absorptive 2DES simulated with the static disorder a,d) $\sigma = 50$ cm^{-1}, b,e) $\sigma = 130$ cm^{-1}, and c,f) $\sigma = 190$ cm^{-1}. The sub-figures (a– c) are simulated at $T = 298$ K, while (d–f) at $T = 77$ K.

extract the TCF, because additional peak emerge due to the large static disorder, as shown in Figure 4c,f. In Figure 6b, a significant fluctuation appears when the static disorder is greater than 80 cm^{-1}, which is more affected than in the case of 298 K.

4. Conclusion

To summarize the main findings of the paper, it is shown that the static disorder has a significant impact on the reliability of the CLS method for obtaining the TCF from 2DES. Specifically, we find that the presence of the static disorder leads to an increase in the steady-state value of the CLS and an inaccurate decay rate of the CLS, as compared to the TCF.

We show that there is a monotonic relation between the steady-state value of the CLS and the amplitude of the static disorder. As the static disorder increases, the steady-state value of the CLS also increases, as shown in Figure 5. According to the simulated data at 77 and 298 K, the relation between the steady-state value and the static disorder is very similar. Due to this monotonic relation, it is possible to obtain the amplitude of the static disorder of the system through the CLS approach.

We also find that the amplitude of the static disorder affects the decay rate of the CLS. When using the CLS method to extract the TCF in the laboratory, the presence of the static disorder can lead to errors in the decay rate, especially in the case with large static disorders. Since we have the correspondent error of the decay

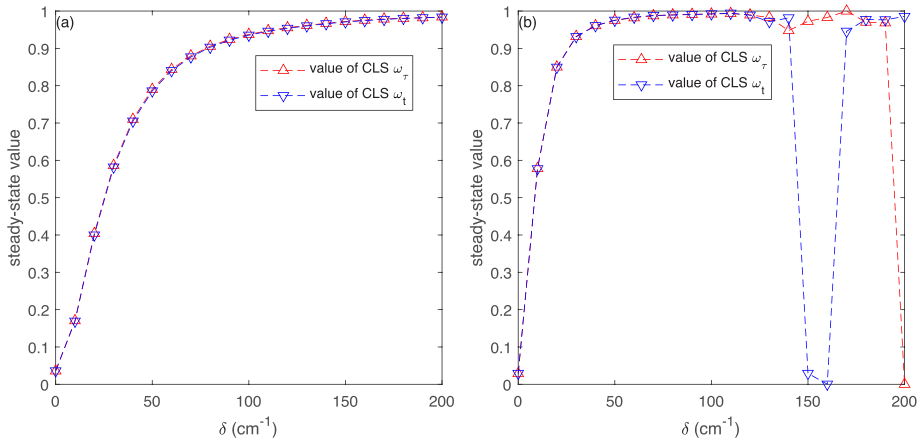

Figure 5. The steady-state value of the CLS at a) $T = 298$ K, b) $T = 77$ K varies with the amplitude of the static disorder. The red (blue) line represents the steady-state value of CLSω_τ (CLSω_t).

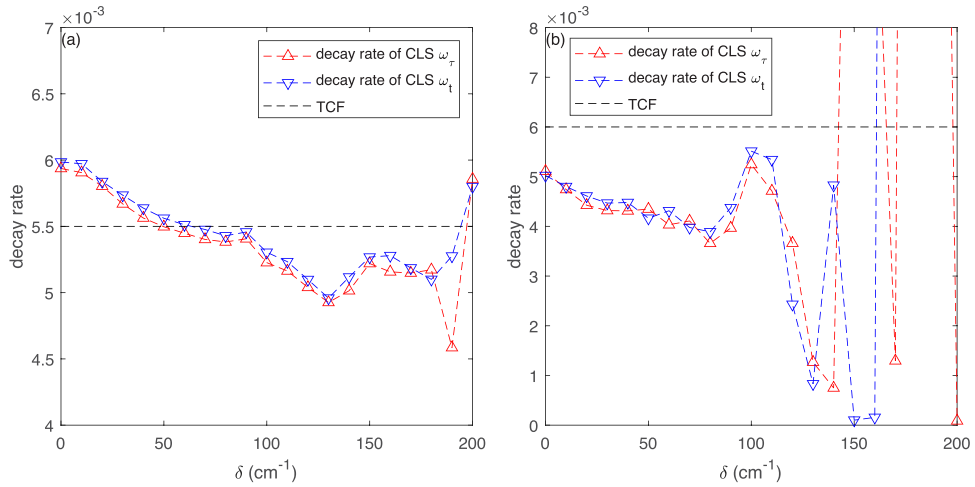

Figure 6. The decay rate of CLS at a) $T = 298$ K, b) $T = 77$ K varies with the amplitude of the static disorder. The red (blue) line represents the change of CLSω_τ (CLSω_t). The black dotted line is the decay rate of the TCF.

rate of the CLS and the amplitude of the static disorder, confer Figure 6, we propose correcting the decay rate of the CLS to attain the decay rate of the TCF.

Our work can provide a correction for the application of the CLS method in actual experiments, where we define the correction $\Delta\gamma = \gamma_{\mathrm{TCF}} - \gamma_{\mathrm{CLS}}$. γ_{TCF} and γ_{CLS} correspond to the decay rates of the TCF and CLS, respectively. In practice, by summing up the obtained decay rate γ with corresponding correction $\Delta\gamma$ according to the static disorder σ, a result which is much closer to that of the TCF can be attained. The corrections for different static disorders are presented in **Tables 3** and **4**.

Table 3. Correction of the decay rate at 298 K.

σ [cm^{-1}]	$\Delta\gamma_t$ ($\times 10^{-4}$fs^{-1})	$\Delta\gamma_\tau$ ($\times 10^{-4}$fs^{-1})
0	−4.855	−4.367
10	−4.723	−4.055
20	−3.380	−3.032
30	−2.354	−1.694
40	−1.379	−0.630
50	−0.610	0.030
60	−0.123	0.520
70	0.236	0.986
80	0.714	1.176
90	0.424	0.939
100	1.956	2.737
110	2.664	3.365
120	4.011	4.604
130	5.414	5.740
140	3.823	4.857
150	2.318	2.806
160	2.208	3.432
170	3.139	3.520
180	4.002	3.275

5. Experimental Section

The 2DES was obtained from the double Fourier transform of the third-order macroscopic polarization signal generated by three laser pulses acting on the system. The 2DES can be theoretically calculated by the response function approach. Afterward, the center line of the 2DES was obtained and the time correlation function was reproduced by the slope of the center line. Hereafter, the two approaches are respectively summarized.

Response Function Theory: Response function is the most commonly-used method for calculating the 2DES, which was developed by S. Mukamel and his collaborators.[40] The 2D spectroscopy can be determined by taking the real part of the Fourier transform of the nonlinear third-order response functions as

$$S^{(3)}(t_3, t_2, t_1) = \left(\frac{-i}{\hbar}\right)^3 \times \langle \mu(t_3)[\mu(t_2), [\mu(t_1), [\mu(0), \rho(-\infty)]]]\rangle \quad (4)$$

where $\hbar$ is the reduced Planck constant, $\mu(t)$ is the dipole operator in the interaction picture, and $\rho(-\infty)$ is the density matrix at thermal

Table 4. Correction of the decay rate at 77 K.

σ [cm^{-1}]	$\Delta\gamma_t$ ($\times 10^{-3}$fs^{-1})	$\Delta\gamma_\tau$ ($\times 10^{-3}$fs^{-1})
0	0.977	0.889
10	1.199	1.258
20	1.389	1.575
30	1.532	1.682
40	1.520	1.689
50	1.837	1.652
60	1.686	1.968
70	2.023	1.891
80	2.110	2.341
90	1.624	2.034
100	0.487	0.756
110	0.658	1.288
120	3.569	2.338
130	5.167	4.732

equilibrium. It can be expanded into four terms and their complex conjugates as

$$\begin{aligned}
R_1(t_3,t_2,t_1) &= |\mu_{01}|^4 e^{-i\omega(t+\tau)} \\
&\times e^{-g(\tau)-g(T_w)-g(t)+g(\tau+T_w)+g(T_w+t)-g(\tau+T_w+t)} \\
R_2(t_3,t_2,t_1) &= |\mu_{01}|^4 e^{-i\omega(t-\tau)} \\
&\times e^{-g(\tau)+g(T_w)-g(t)-g(\tau+T_w)-g(T_w+t)+g(\tau+T_w+t)} \\
R_3(t_3,t_2,t_1) &= |\mu_{01}|^4 e^{-i\omega(t-\tau)} \\
&\times e^{-g(\tau)+g(T_w)-g(t)-g(\tau+T_w)-g(T_w+t)+g(\tau+T_w+t)} \\
R_4(t_3,t_2,t_1) &= |\mu_{01}|^4 e^{-i\omega(t+\tau)} \\
&\times e^{-g(\tau)-g(T_w)-g(t)+g(\tau+T_w)+g(T_w+t)-g(\tau+T_w+t)}
\end{aligned} \tag{5}$$

where $t_1 = \tau$, $t_2 = \tau + T_w$, and $t_3 = \tau + T_w + t$ are the delay times, ω is the transition frequency between the ground state $|0\rangle$ and the excited state $|1\rangle$, $\mu_{01} = \langle 0|\mu|1\rangle$ is the transition dipole between the two states. And $g(t)$ is the line-shape function,[40] which is obtained from the double integration of the TCF as

$$g(t) = \frac{1}{2}\int_0^t \mathrm{d}t' \int_0^{t'} \mathrm{d}t'' C(t'') \tag{6}$$

Generally, the TCF reads[40]

$$\begin{aligned}
C(t) &\equiv \int \mathrm{d}\omega J(\omega)\left[\coth\left(\frac{\beta\omega}{2}\right)\cos(\omega t) - i\sin(\omega t)\right] \\
&\equiv C'(t) + iC''(t)
\end{aligned} \tag{7}$$

where $C'(t)$ and $C''(t)$ are respectively the real and imaginary parts of the TCF, $J(\omega)$ is the spectral density characterizing the system-bath interaction, $\beta = 1/k_B T$ is the inverse temperature with k_B and T being the Boltzmann constant and the temperature, respectively. The real and imaginary parts of the TCF have corresponding relations. When we have the imaginary part, we also know the real part and vice versa, that is

$$C''(t) = \tan\left(\frac{\beta\hbar}{2}\frac{\mathrm{d}}{\mathrm{d}t}\right)C'(t) \tag{8}$$

which will be proven in Supporting Information.

Center-Line Slope: In the approach of the center-line slope, two approximations were made to obtain the TCF, that is, $C(t) = \delta(t)/T_2 + \Delta^2 \exp(-t/\tau_d)$.[34] First of all, the homogeneous line width was set to zero, that is, $1/T_2 = 0$. This approximation ensured that the motionally-narrowed component of $C(t)$ was no longer present. In addition, under short-time approximation, the line-shape function was expanded to the second order of the coherence times, that is, τ and t, as

$$g(t) = \Delta^2\tau_d t + \Delta^2\tau^2(e^{-t/\tau_d} - 1) \approx \frac{\Delta^2 t^2}{2} \tag{9}$$

where the short-time approximation assumes slow spectral dispersion, that is, $\Delta\tau_d \gg 1$.

Subsequently, the absorptive line shape can be written as

$$\begin{aligned}
R^g(\omega_\tau, T_w, \omega_t) &= \frac{2\pi}{\sqrt{C^2(0) - C^2(T_w)}} \\
&\times \exp\left(-\frac{C(0)(\omega_t^2 + \omega_\tau^2) - 2C(T_w)\omega_\tau\omega_t}{2(C^2(0) - C^2(T_w))}\right)
\end{aligned} \tag{10}$$

For a specific ω_t, we can obtain the maximum by calculating the derivative with respect to ω_τ as

$$\begin{aligned}
&\frac{\partial R^g(\omega_\tau, T_w, \omega_t)}{\partial\omega_\tau}\Big|_{\omega_\tau=\omega_\tau^{\max}} \\
&= \frac{-C(0)\omega_\tau + C(T_w)\omega_t}{C^2(0) - C^2(T_w)} \times R^g(\omega_\tau, T_w, \omega_t) = 0
\end{aligned} \tag{11}$$

The center line is the line connecting the maxima for different ω_t. The CLS is the slope of the center line, that is

$$\mathrm{CLS}\omega_t(T_w) = \frac{\mathrm{d}\omega_\tau^{\max}(\omega_t)}{\mathrm{d}\omega_t} = \frac{C(T_w)}{C(0)} \tag{12}$$

Alternatively, the CLS can be obtained in a similar way as

$$\mathrm{CLS}\omega_\tau(T_w) = \frac{\mathrm{d}\omega_t^{\max}(\omega_\tau)}{\mathrm{d}\omega_\tau} = \frac{C(T_w)}{C(0)} \tag{13}$$

where the maximum is determined by

$$\begin{aligned}
&\frac{\partial R^g(\omega_\tau, T_w, \omega_t)}{\partial\omega_t}\Big|_{\omega_t=\omega_t^{\max}} \\
&= \frac{-C(0)\omega_t + C(T_w)\omega_\tau}{C^2(0) - C^2(T_w)} \times R^g(\omega_\tau, T_w, \omega_t) = 0.
\end{aligned} \tag{14}$$

Note that the CLS method is based on the response function, which treats all excitation pulses as delta pulses. Furthermore, several approximations were employed, such as the short-time approximation, omitting the homogeneous term and assuming the TCF to be real. Therefore, it is quite natural to question the validity of the CLS approach under a more realistic condition, for example, employing it in the 2DES in the visible-frequency domain at low temperatures.

Supporting Information

Supporting Information is available from the Wiley Online Library or from the author.

Acknowledgements

The authors thank stimulating discussions with H. Dong, W.-T. He, and N.-N. Zhang. This work is supported by Beijing Natural Science Foundation under Grant No. 1202017 and the National Natural Science Foundation of China under Grant Nos. 11674033, 11505007, and Beijing Normal University under Grant No. 2022129. Y.-C.C. thanks the Ministry of Science and Technology, Taiwan (Grants No. MOST 109-2113-M-002-004 and No. MOST 109-2113-M-001-040), and National Taiwan University (Grant No. 111L894603) for financial support.

Conflict of Interest

The authors declare no conflict of interest.

Data Availability Statement

The data that support the findings of this study are available from the corresponding author upon reasonable request.

Keywords

2D electronic spectroscopy, center-line slope, static disorder, time correlation function

Received: June 3, 2023
Revised: August 4, 2023
Published online:

[1] E. Collini, G. D. Scholes, *Science* **2009**, *323*, 369.
[2] B.-X. Wang, M.-J. Tao, Q. Ai, T. Xin, N. Lambert, D. Ruan, Y.-C. Cheng, F. Nori, F.-G. Deng, G.-L. Long, *npj Quantum Inf.* **2018**, *4*, 52.
[3] Y. Song, S. N. Clafton, R. D. Pensack, T. W. Kee, G. D. Scholes, *Nat. Commun.* **2014**, *5*, 4933.
[4] A. De Sio, F. Troiani, M. Maiuri, J. Réhault, E. Sommer, J. Lim, S. F. Huelga, M. B. Plenio, C. A. Rozzi, G. Cerullo, E. Molinari, C. Lienau, *Nat. Commun.* **2016**, *7*, 13742.
[5] E. Harel, G. S. Engel, *Proc. Natl. Acad. Sci. USA* **2012**, *109*, 706.
[6] S. Yue, Z. Wang, X. Leng, R.-D. Zhu, H.-L. Chen, Y.-X. Weng, *Chem. Phys. Lett* **2017**, *683*, 591.
[7] A. F. Fidler, V. P. Singh, P. D. Long, P. D. Dahlberg, G. S. Engel, *J. Phys. Chem. Lett.* **2013**, *4*, 1404.
[8] E. E. Ostroumov, R. M. Mulvaney, R. J. Cogdell, G. D. Scholes, *Science* **2013**, *340*, 52.
[9] A. F. Fidler, V. P. Singh, P. D. Long, P. D. Dahlberg, G. S. Engel, *Nat. Commun.* **2014**, *5*, 3286.
[10] T. R. Calhoun, N. S. Ginsberg, G. S. Schlau-Cohen, Y.-C. Cheng, M. Ballottari, R. Bassi, G. R. Fleming, *J. Phys. Chem. B* **2009**, *113*, 16291.
[11] E. Collini, C. Y. Wong, K. E. Wilk, P. M. G. Curmi, P. Brumer, G. D. Scholes, *Nature* **2010**, *463*, 644.
[12] Q. Ai, Y. J. Fan, B. Y. Jin, Y. C. Cheng, *New J. Phys.* **2014**, *16*, 053033.
[13] R.-D. Zhu, J.-D. Zou, Z. Wang, H.-L. Chen, Y.-X. Weng, *J. Phys. Chem. A* **2020**, *124*, 9333.
[14] Y.-C. Cheng, H. Lee, G. R. Fleming, *J. Phys. Chem. A* **2007**, *111*, 9499.
[15] G. Panitchayangkoon, D. Hayes, K. A. Fransted, J. R. Caram, E. Harel, J.-Z. Wen, R. E. Blankenship, G. S. Engel, *Proc. Natl. Acad. Sci. USA* **2010**, *107*, 12766.
[16] X. Leng, Y.-M. Yan, R.-D. Zhu, K. Song, Y.-X. Weng, Q. Shi, *J. Phys. Chem. B* **2018**, *122*, 4642.
[17] D. M. Monahan, L. Guo, J. Lin, L. T. Dou, P. D. Yang, G. R. Fleming, *J. Phys. Chem. Lett.* **2017**, *8*, 3211.
[18] J. M. Richter, F. Branchi, F. Valduga de Almeida Camargo, B. D. Zhao, R. H. Friend, G. Cerullo, F. Deschler, *Nat. Commun.* **2017**, *8*, 376.
[19] D. B. Turner, Y. Hassan, G. D. Scholes, *Nano Lett.* **2012**, *12*, 880.
[20] E. Cassette, R. D. Pensack, B. Mahler, G. D. Scholes, *Nat. Commun.* **2015**, *6*, 6086.
[21] T. Stoll, F. Branchi, J. Réhault, F. Scotognella, F. Tassone, I. Kriegel, G. Cerullo, *J. Phys. Chem. Lett.* **2017**, *8*, 2285.
[22] J. R. Caram, H.-B. Zheng, P. D. Dahlberg, B. S. Rolczynski, G. B. Griffin, A. F. Fidler, D. S. Dolzhnikov, D. V. Talapin, G. S. Engel, *J. Phys. Chem. Lett.* **2014**, *5*, 196.
[23] G. Nardin, G. Moody, R. Singh, T. M. Autry, H.-B. Li, F. Morier-Genoud, S. T. Cundiff, *Phys. Rev. Lett.* **2014**, *112*, 046402.
[24] S. D. Park, D. Baranov, J. Ryu, B. Cho, A. Halder, S. Seifert, S. Vajda, D. M. Jonas, *Nano Lett.* **2017**, *17*, 762.
[25] E. Romero, R. Augulis, V. I. Novoderezhkin, M. Ferretti, J. Thieme, D. Zigmantas, R. van Grondelle, *Nat. Phys.* **2014**, *10*, 676.
[26] H.-G. Duan, V. I. Prokhorenko, E. Wientjes, R. Croce, M. Thorwart, R. J. Miller, *Sci. Rep.* **2017**, *7*, 12347.
[27] Y.-C. Cheng, G. R. Fleming, *Annu. Rev. Phys. Chem* **2009**, *60*, 241.
[28] G. S. Engel, T. R. Calhoun, E. L. Read, T.-K. Ahn, T. Mančal, Y.-C. Cheng, R. E. Blankenship, G. R. Fleming, *Nature* **2007**, *446*, 782.
[29] A. Perdomo-Ortiz, J. R. Widom, G. A. Lott, A. Aspuru-Guzik, A. H. Marcus, *J. Phys. Chem. B* **2012**, *116*, 10757.
[30] P. Malý, T. Mančcal, *J. Phys. Chem. Lett.* **2018**, *9*, 5654.
[31] D. F. Liang, H. B. Li, *J. Chem. Phys.* **2021**, *154*, 214301.
[32] W. Kuehn, K. Reimann, M. Woerner, T. Elsaesser, R. Hey, U. Schade, *Phys. Rev. Lett.* **2011**, *107*, 067401.
[33] W. Kuehn, K. Reimann, M. Woerner, T. Elsaesser, R. Hey, *J. Phys. Chem. B* **2011**, *115*, 5448.
[34] K. Kwak, S. Park, I. J. Finkelstein, M. D. Fayer, *J. Chem. Phys.* **2007**, *127*, 124503.
[35] K. Kwak, D. E. Rosenfeld, M. D. Fayer, *J. Chem. Phys.* **2008**, *128*, 204505.
[36] I. J. Finkelstein, H. Ishikawa, S. Kim, A. M. Massari, M. D. Fayer, *Proc. Natl. Acad. Sci. USA* **2007**, *104*, 2637.
[37] C. Fang, J. D. Bauman, K. Das, A. Remorino, E. Arnold, R. M. Hochstrasser, *Proc. Natl. Acad. Sci. USA* **2008**, *105*, 1472.
[38] S. Park, M. D. Fayer, *Proc. Natl. Acad. Sci. USA* **2007**, *104*, 16731.
[39] H. Ishikawa, S. Kim, K. Kwak, K. Wakasugi, M. D. Fayer, *Proc. Natl. Acad. Sci. USA* **2007**, *104*, 19309.
[40] S. Mukamel, *Principles of Nonlinear Optics and Spectroscopy*, Oxford University Press, New York **1999**.
[41] Y.-X. Weng, H.-L. Chen, *Ultrafast Spectroscopy-Principles and Techniques*, Chemical Industry Press, Shanghai **2013**.
[42] F. Šanda, V. Perlík, C. N. Lincoln, J. Hauer, *J. Phys. Chem. A* **2015**, *119*, 10893.
[43] D. J. Hoffman, M. D. Fayer, *J. Phys. Chem. A* **2020**, *124*, 5979.
[44] V. Butkus, H. Dong, G. R. Fleming, D. Abramavicius, L. Valkunas, *J. Phys. Chem. Lett.* **2016**, *7*, 277.
[45] H. Dong, G. R. Fleming, *J. Phys. Chem. B* **2014**, *118*, 8956.
[46] C. Meier, D. J. Tannor, *J. Chem. Phys.* **1999**, *111*, 3365.
[47] M. Abramowitz, I. A. Stegun, *Handbook of Mathematical Functions with Formulas, Graphs, and Mathematical Tables*, Dover, New York **1964**.
[48] J. Mayer, K. Khairy, J. Howard, *Am. J. Phys.* **2010**, *78*, 648.
[49] F. Dyson, *Nature* **2004**, *427*, 297.